Solubility isotherms of hydrogen in epitaxial Nb(110) films

G. Song, M. Geitz, A. Abromeit, and H. Zabel
Ruhr-Universität Bochum, Fakultät für Physik und Astronomie, Institut für Experimentalphysik/Festkörperphysik, D-44780 Bochum, Germany
(Received 6 May 1996)

The solubility isotherms of hydrogen in epitaxial Nb(110) films have been determined via *in situ* x-ray lattice-parameter measurements. The Nb films were grown by molecular-beam epitaxial techniques on $Al_2O_3(11\bar{2}0)$ substrates with thicknesses ranging from 32 to 527 nm. All isotherms can be well described by the standard expression for the solubility of a monatomic lattice gas. Aside from the metal-hydrogen interaction, which appears to be bulklike, all other properties exhibit a strong thickness dependence, including the hydrogen-hydrogen interaction, the critical temperature for the α-α' transition, and the maximum lattice-parameter change that can be reached in saturation. For the critical temperature we find a scaling with the film thickness, which most likely is due to the elastic boundary condition provided by the rigid substrate. The clamping of the epitaxial film to the substrate hinders critical fluctuations of macroscopic hydrogen density modes from developing, thereby lowering the critical temperature for the α-α' transition. [S0163-1829(96)05443-4]

I. INTRODUCTION

Solubility isotherms of hydrogen in metals belong to the fundamental properties from which other physical parameters can be derived. For instance, the metal-hydrogen and hydrogen-hydrogen interactions, as well as the formation enthalpies for different phases and phase transitions, follow from the isotherms. For bulk metals the hydrogen solubility isotherms are well established.[1] In recent years, interest has turned to the properties of H in thin films and superlattices.[2] Early measurements of the H solubility in Nb and Pd films provided conflicting results.[3,4] This is due in part to the film deposition technique used, and in part to the determination of the hydrogen concentration on an absolute scale. Classical methods such as gravimetric and volumetric methods are difficult to apply because of the small quantities of hydrogen in the thin films. More recently, Weidinger and his group reported a solubility study of H in epitaxial Nb(110) films of different thickness.[5] The H concentration was determined *in situ* by the resonant nuclear reaction $^1H(^{15}N,\alpha\gamma)^{12}C$ method. From these measurements they concluded that the metal-hydrogen interaction is essentially the same as in the bulk, and that the H-H interaction is reduced by at least a factor of 2. The isotherms were limited with respect to the maximum hydrogen concentration that could be reached, because of vacuum requirements in the accelerator environment, allowing pressures not higher than about 10^2 Pa. In another recent study the isotherms were determined for sputtered Nb films on glass substrates using electrical resistivity measurements.[6] The absolute concentration was calibrated volumetrically by hot extraction. In this study no clear dependence of the isotherms on the film thickness was observed, and the authors concluded that the important parameter for the isotherms is not the film thickness but the ratio between the film thickness and the particle size. When this parameter exceeds unity, the dependence of the isotherms on the film thickness becomes less pronounced.

In the present study we used x-ray diffraction techniques to measure the lattice-parameter change as a function of the external hydrogen pressure. This provides very accurate solubility isotherms on a relative scale of volume expansion. The conversion to hydrogen concentrations must then be carried out by another independent calibration measurement. Here we will report on solubility isotherms of hydrogen in Nb epitaxial films grown in the (110) direction with different thicknesses on $Al_2O_3(11\bar{2}0)$ substrates. The main motivation for this work is the analysis of the thickness dependence of the hydrogen solubility in Nb, and the need for understanding the effect the elastic boundary condition has on the hydrogen-metal and hydrogen-hydrogen interaction. The work of the Weidinger group points to a strong dependence on the Nb film thickness.[5] Here we like to extend the isotherms to higher H concentrations and to different film thicknesses. Furthermore, we aim to understand the effect of the boundary condition and the film thickness on the critical temperature for the α-α' phase transition. The phase transition of hydrogen in metals has been shown to depend strongly on the shape of the sample.[7] The highest critical temperature is referred to as the incoherent or strain free critical temperature, which is independent of the sample shape. All other excitations of macroscopic hydrogen density modes are uniquely related to a set of spinodal temperatures lying below the incoherent critical temperature. Macroscopic hydrogen density modes have been observed in thin Nb plates.[8,9] For instance, a thin Nb disk loaded with the critical hydrogen concentration will bend according to the shape of a spherical shell by lowering the temperature through the critical point. For a film on a rigid substrate the bending mode is suppressed. This elastic boundary condition is expected to affect the critical fluctuations and subsequently the critical temperature. In the extreme case only microscopic modes which propagate parallel to the film plane and which are insensitive to the sample shape may be excited at much lower temperatures.[10]

II. SAMPLE PREPARATION AND EXPERIMENTAL PROCEDURES

We have grown single-crystalline Nb(110)-oriented films by molecular-beam epitaxy (MBE) on $Al_2O_3(11\bar{2}0)$ substrates. The procedure for growing Nb films of high structural quality is well established, and has been reported in several places.[11,12] The sapphire substrates had a miscut of less than 1°, and were of high crystalline quality with mosaicities between 0.002° and 0.006°. The Nb deposition was carried out in a Riber EVA 32 MBE machine under ultrahigh vacuum (UHV) conditions (base pressure better than 2×10^{-9} Pa) working pressure 10^{-8} Pa. After chemically etching and rinsing in acetone and isopropanol, the substrates were transferred into the UHV system. Final cleaning was achieved by sputtering for 30 min with Ar^+ (600 eV, 1 $\mu A/cm^2$) at 500 °C followed by annealing for 1 h at 1100 °C. Nb was evaporated with an electron beam gun at a substrate temperature of 900 °C. *In situ* reflection high-energy electron diffraction confirmed a very smooth growth of the Nb films.

Afterwards a Pd film of about D_{Pd} = 2-nm thickness was deposited on the Nb surface with a (111) orientation. This enhances the catalytic dissociation of hydrogen molecules at the surfaces and at the same time hinders the oxidation of the Nb surface. Using Pd cap layers on Nb, isotherms can be measured to much lower temperatures than would be possible otherwise. Several films with thicknesses of D_{Nb} = 32, 78, 95, 140, and 527 nm were prepared in the fashion described above. The thicknesses of the first four samples were determined via small angle x-ray reflectivity measurements. For the sample with the highest thickness, the resolution of our diffractometer set up was not sufficient. Therefore, we determined the thickness of this sample by Rutherford backscattering methods using $^4_2He^{2+}$ particles. The x-ray experiments were carried out using Mo-$K_{\alpha1}$ radiation monochromated by a Si(110) reflection in the incident beam. The x-ray setup was already described in previous papers.[17] For the hydrogen loading an x-ray furnace equipped with Al windows was used. After pumping down to about 10^{-6} Pa, the sample was exposed to hydrogen gas of variable pressure from a gas bottle containing very pure hydrogen gas (99.999 %). The hydrogen pressure was measured by a Bayard-Alpert ion gauge for pressures from 10^{-8} to 10^{-1} Pa, and two capacitive transducers with ranges from 2×10^{-2} to 2×10^{2} Pa and from 10 to 10^5 Pa, respectively.

III. STRUCTURAL CHARACTERIZATIONS

The epitaxial relation between Nb and sapphire is well known, and has been described in several places. For completeness, the epitaxial relation for our orientation shall be quoted here:[13,14]

$$Al_2O_3 \quad Nb$$

$$[11\bar{2}0]\|[1\bar{1}0]$$

$$[0001]\|[111]$$

$$[\bar{1}100]\|[11\bar{2}]$$

In Fig. 1 a typical refelectivity scan of the 95-nm-thick sample is shown before and after hydrogen loading. The reflectivity exhibits low-frequency oscillations due to the 11-nm-thick Pd cap layer and high-frequency oscillations from the Nb film. After finishing a complete solubility cycle, the roughness of the interfaces is slightly increased, in particular at the Nb/Pd interface. The solid lines show fits to the data points according to the Parratt formalism for specular reflection.[15] The roughness at each interface is included as Gaussian fluctuations.[16] The best-fit paramaters are listed in Table I.

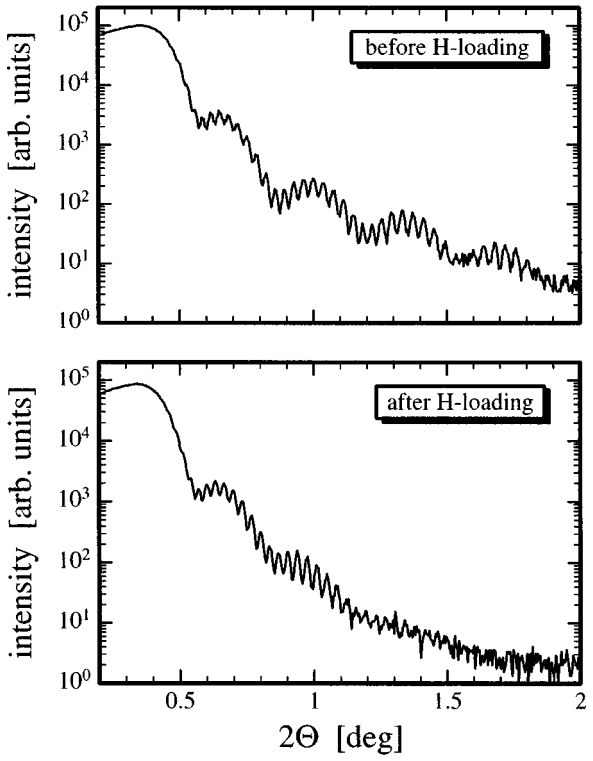

FIG. 1. Small-angle x-ray reflectivity measurements of a 95-nm-thick Nb(110) film on $Al_2O_3(11\bar{2}0)$ substrate capped with a 11-nm-thick Pd overlayer. The narrow oscillations are due to the Nb film, and the wide oscillations to the Pd cap layer. The reflectivity meausrements are shown for the sample immediately after growth (top panel) and after hydrogen uptake to high concentrations (bottom panel).

More pronounced are the changes of the coherent crystal structure as observed at the (110) Bragg point. Figure 2

TABLE I. Structural parameters of some of the Nb(110) films used for the hydrogen solubility isotherms.

D_{Nb}	D_{Pd}	Coherence length		Mosaicity	
		before	after	before	after
(nm)	(nm)	(nm)	(nm)	(deg)	(deg)
32	3.3	30.0	14.8	0.030	0.5
78	3.3	57.7	37.2	0.029	0.8
95	11.0	62.3	24.8	0.012	0.5
140	2.0	92.0	32.0	0.026	1.5
527	11.7	68.1	50.4	0.064	1.0

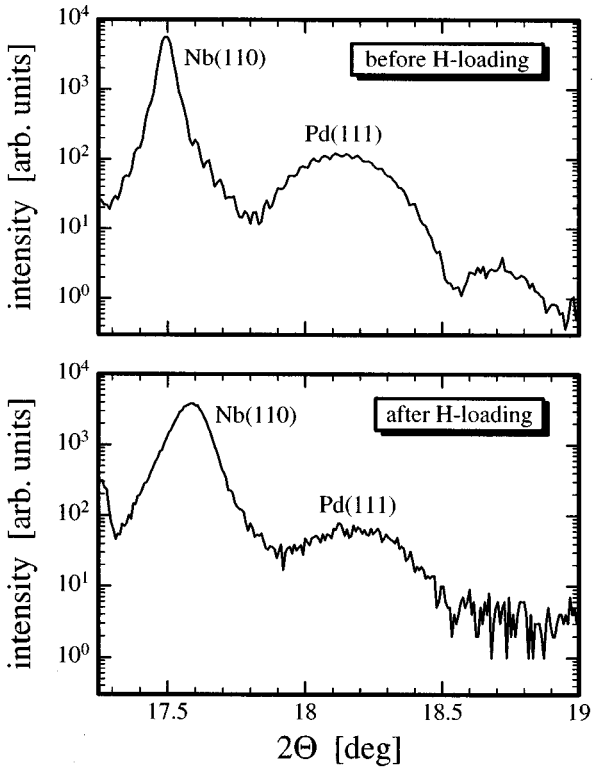

FIG. 2. Bragg scans in the radial direction normal to the film plane before and after hydrogen loading of the same film as described in Fig. 1. The Nb(110) and Pd(111) Bragg peaks are plotted on a logarithmic scale. Both peaks show thin-film oscillations before hydrogen loading which become damped out after hydrogen exposure.

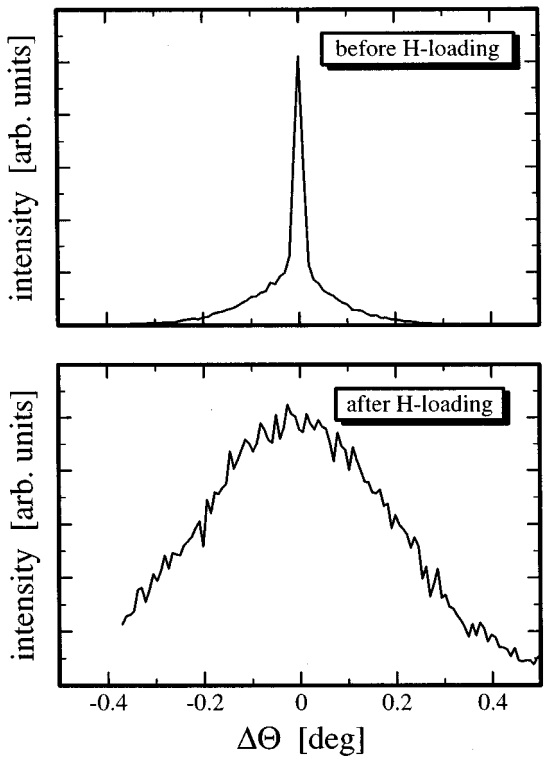

FIG. 3. Rocking scan through the Nb(110) Bragg peak before (top panel) and after hydrogen loading (bottom panel) of the same sample shown in Figs. 1 and 2. Before hydrogen loading the Bragg peak exhibits a double line shape with a very narrow central component typical for highly coherent epitaxial growth. Due to elastic strains in the film the coherent structure breaks down after hydrogen loading up to high hydrogen concentrations.

reproduces radial Bragg scans of the same sample before and after hydrogen loading. Thin film thickness or Laue oscillations can be observed for both the pristine Nb and Pd films. However, after hydrogen loading these oscillations become smeared out due to a continuous loss of structural coherence. Even more drastic is the change of the mosaicity. Before hydrogen exposure the rocking curve of the Nb(110) reflection, as shown in Fig. 3 (top panel), exhibits a double line shape typical of highly coherent epitaxial films.[17–19] The sharp component has a width of 0.01°, whereas the broad component has a width of 0.5°. It has been shown in the past that small amounts of hydrogen can considerably improve the width of the sharp component.[18] The sharpening is most likely due to a hydrogen-assisted cold annealing effect of residual epitaxial strains in the film. Here we are dealing with much higher hydrogen concentrations, which have a detrimental effect on the mosaicity. After a complete solubility cycle the mosaicity increases to at least 1° (see Fig. 3, bottom panel), and in some cases to even much higher values. Thus at higher concentrations the structural coherence is considerably reduced, and the film breaks up into small crystallites including an increasing number of grain boundaries between them. The increased mosaicity after hydrogen exposure is irreversible. In this state the Nb film on sapphire is highly textured but still not a polycrystal. Then we expect the lattice to expand nearly isotropically, as in bulk samples with free surfaces. The H-H interaction should not be affected very much by the presence of dislocations and grain boundaries, since the range of the elastic interaction is typically much larger than the grain sizes. More important than the mosaicity and the grain size for the H-H interaction is the elastic boundary condition provided by the rigid sapphire substrate.

IV. SOLUBILITY ISOTHERMS

Figure 4 reproduces the solubility isotherms for hydrogen in Nb(110) films grown epitaxially on $Al_2O_3(1120)$ substrates. The external hydrogen pressure p_{H_2} is plotted as a function of the lattice parameter change $(\Delta a/a)_H = \varepsilon_H$ for several temperatures and pressures, and for several film thicknesses. Because of the Pd cap layer the oxygen barrier for hydrogen diffusion into the bulk is eliminated, allowing it to follow the isotherms to rather low temperatures. The isotherms as shown in Fig. 4 were measured with increasing pressure for practical reasons. The hysteresis between increasing and decreasing pressures is not very large. However, the time constants for reaching equilibrium conditions are considerably larger for decreasing than for increasing pressures. The time constants also become very large in the plateau region when approaching the critical temperature for the α-α' phase transition. This is due to the critical slowing down of the hydrogen mobility close to the critical point. In

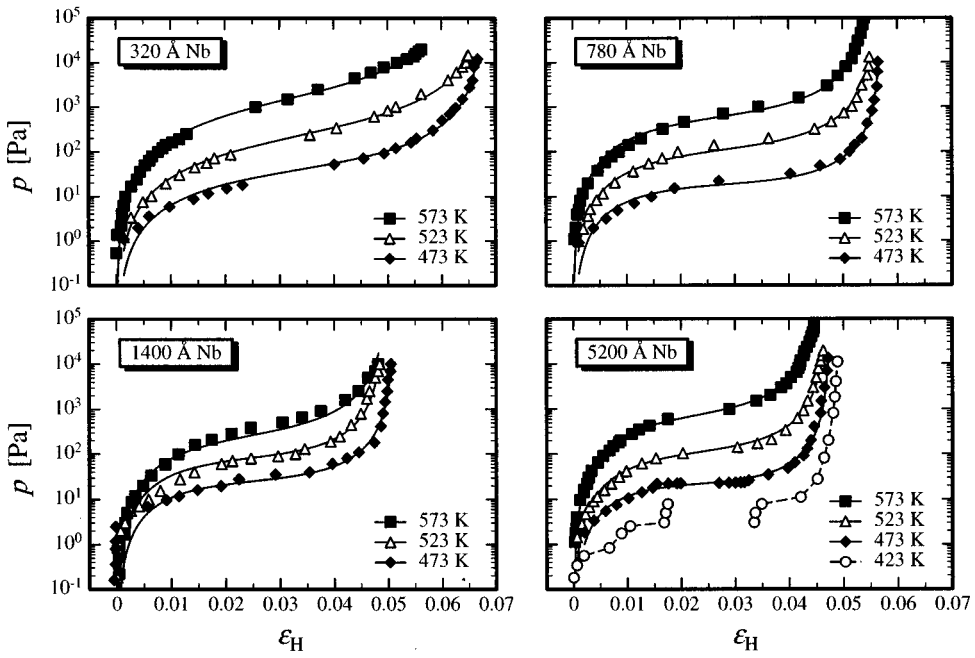

FIG. 4. X-ray measurements of the solubility isotherms for hydrogen in Nb thin films. p_{H_2} is the external hydrogen pressure, and ε is the relative lattice parameter change. The dashed lines are fits to the data points with the expression in Eq. (21). In the case of the 527-nm-thick film the isotherm at 423 K cuts through the α-α' coexistence region. For this isotherm no fit is provided.

the case of the 527-nm thick Nb film, the lowest isotherm at 150 °C enters the two-phase region, and the coexistence of the two phases α and α' can be clearly seen by a split up of the Bragg reflections into two peaks, as demonstrated in Fig. 5. Their intensities follow the well-known lever rule.

In Fig. 5 the isotherms at 523 K are compared for different film thicknesses. It is easy to see that the maximum lattice parameter change $\varepsilon_{H,max}$, as well as the slope of the isotherms at the inflection points, depend on the film thickness. The position of the inflection point defines the critical hydrogen concentration $c_{H,c}$, and the slope of the isotherm at the inflection point becomes zero at the critical temperature T_c. The thickness dependence of both parameters is well pronounced for the thin films and is demonstrated here for the first time, to our knowledge. We will come back to this point in the discussion section. All solid lines are fits to the measured isotherms using an expression for the solubility isotherm discussed in Sec. IV.

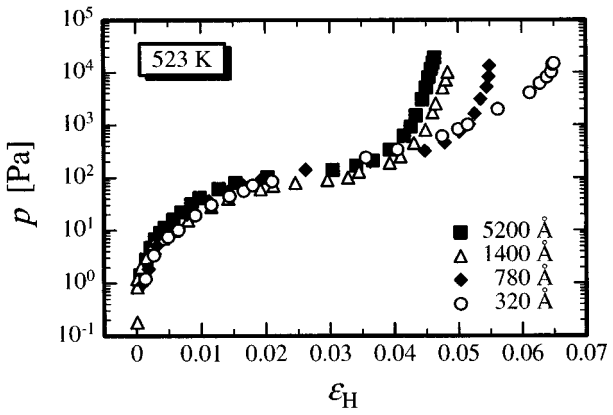

FIG. 5. The solubility isotherms at 523 K are compared for the different Nb film thicknesses. The maximum lattice parameter change and the slope at the inflection point of the isotherms strongly depend on the film thickness.

V. DISCUSSION

A. Hydrogen concentration and lattice expansion

As mentioned previously, in this study we measured the external hydrogen pressure p_{H_2} as a function of the relative lattice parameter change ε_H and not as a function of the hydrogen concentrations c_H. In the bulk and for isotropic expansion the relation between ε_H and c_H is well established;

$$(\Delta V/V)_H = 3\varepsilon_H = f c_H, \tag{1}$$

where $(\Delta V/V)_H$ is the relative volume change, and the proportionality factor f is given by the ratio between the local volume expansion per hydrogen atom dissolved in the metal matrix and the atomic wolume of the metal atom,

$$f = \frac{\Delta v}{\Omega}. \tag{2}$$

With $\Omega = a^3/2 = 18\times 10^3$ nm^3 and $\Delta v = 3.13\times 10^3$ nm^3 for H in bulk Nb, $f = 0.174$. In the bulk, f is a constant even up to very high hydrogen concentrations.[20] Therefore, for bulk investigations the lattice parameter change can safely be used for measuring hydrogen concentrations. However, for thin films the situation is more complex. At small concentrations, a one-dimensional expansion perpendicular to the film plane has been observed without any lattice parameter changes in the film plane.[21] In this case,

$$(\Delta V/V)_H = \varepsilon_H = \overline{f} c_H. \tag{3}$$

Standard elasticity theory relates f and $\overline{f}$, taking into account the Poisson reaction in the out-of-plane direction from the suppression of in-plane expansion. Then

$$\overline{f} = \gamma f,$$

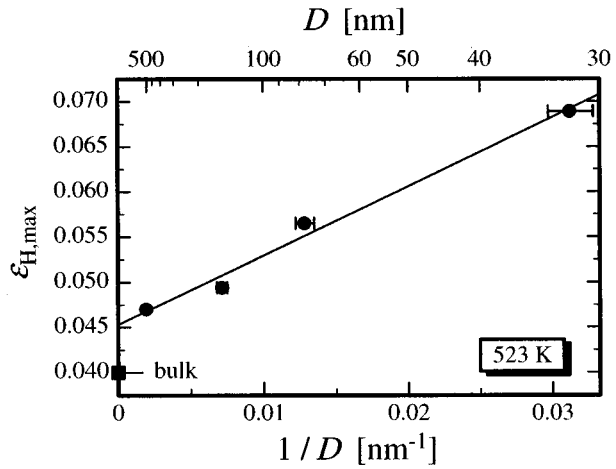

FIG. 6. The maximum lattice parameter change in saturation is plotted a function of the inverse film thickness. At $1/D=0$ the bulk value known from the literature is shown.

$$\gamma=\frac{1}{3}\left[1+\left(\frac{C_{11}+3C_{12}-2C_{44}}{C_{11}+C_{12}+2C_{44}}\right)\right]. \tag{4}$$

Here γ is given for the (110) orientation of the Nb film, and $C_{i,j}$ are the elastic constants. Inserting the known values for the elastic constants we obtain $\gamma=0.78$, such that $f=0.136$. This calculated f value is in stark variance to the reported experimental value of 0.53, being different by almost a factor of 4.[22] This unusually large uniaxial expansion holds for hydrogen concentrations up to about 2%, beyond which it breaks down.[22] For higher concentrations, dislocations are formed, and the film loses the high structural coherence, as already described in Sec. III. For these higher H concentrations the lattice expansion is expected to relax to values closer to the three-dimensional bulk behavior. Thus, loading a pristine Nb film with hydrogen, a nonlinear lattice expansion as a function of the hydrogen should occur. However, to our knowledge this experiment has not been carried out convincingly up to date. After charging and discharging a Nb film several times, the structural coherence is lost, and even a thin film should then expand more like a bulk sample. Nevertheless, for thin epitaxial films the conversion from relative lattice parameter changes to hydrogen concentrations should always be done with some caution.

For the thinnest sample of 32-nm Nb, we have measured lattice parameter changes as high as 6.5% (see Fig. 6). Assuming bulk properties, this expansion corresponds to a hydrogen concentration of about 112%, which is almost twice as large as observed in the bulk. We have also carried out neutron reflectivity measurements on the same sample to determine the hydrogen concentration independently. These results will be reported elsewhere.[23] It should, however, be mentioned here that preliminary analysis indicates a maximum hydrogen concentration on the order of only 95%. This is still much higher than in the bulk, but somewhat smaller than estimated using the bulk conversion factor f. This discrepancy indicates that the f coefficient in thin Nb films may still be a bit larger than for bulk samples, in spite of cycling the isotherms for several times. On the other hand, we can exclude nonlinearities of the lattice expansion along a measured solubility isotherm by noting that the inflection point of the isotherms are at the same time also the centers of symmetry; that is,

$$c_{\mathrm{H},c}=c_{\mathrm{H,max}}/2=r/2 \tag{5}$$

or, in terms of lattice parameter changes,

$$\varepsilon_{\mathrm{H},c}=\varepsilon_{\mathrm{H,max}}/2. \tag{6}$$

In conclusion, for the present investigation of hydrogen solubility isotherms in thin Nb films the f factor is most likely close to the bulk value, indicating that the expansion is more or less isotropic. This is achieved by loading the film with the maximum hydrogen concentration several times, and then carefully determining a particular isotherm.

B. Maximum hydrogen concentration

Obviously $\varepsilon_{\mathrm{H,max}}$ is largest for the thinnest sample, and decreases with increasing sample thickness. In Fig. 6 we plotted $\varepsilon_{\mathrm{H,max}}$ as a function of the inverse sample thickness D. The bulk value at $1/D=0$ is calculated from the bulk isotherms using the bulk conversion factor $f=0.174$. Clearly, the maximum lattice parameter change $\varepsilon_{\mathrm{H,max}}$ in thin films depends inversely on the sample thickness. This is a rather surprising result. According to this plot, the 527-nm-thick film comes close to bulk properties.

$1/D$ dependencies are also observed, for instance, for magnetic anisotropies in magnetic thin films.[24] There they are due to a surface contribution of the anisotropy energy. In our case surface contributions to the lattice expansion (f-factor) and/or hydrogen concentration (r-factor) may also be responsible for the increased $\varepsilon_{\mathrm{H,max}}$ in thin films. It is, however, unlikely that the Pd cap layer induces this surface term, since the hydrogen solubility in Pd is much smaller than in Nb.

Hjörvarsson *et al.* also observed a maximum H concentration in Mo/V superlattices which depends inversely on the V layer thickness.[25] However, in contrast to our single Nb films, the H concentration becomes reduced with decreasing V layer thickness. This was explained by a depletion zone of hydrogen close to the Mo/V interface due to an electronic spillover from Mo to V, which in turn reduces the H solubility. The proximity effect is limited to about three V monolayers next to the Mo/V interface. In contrast, the enhanced hydrogen concentration in thin Nb films is observed over much thicker films. Therefore, in our case a proximity effect from the hybridization of the Nb and Pd bands at the interface is quite unlikely the cause for the $1/D$ dependence of $\varepsilon_{\mathrm{H,max}}$.

It should also be noted that $\varepsilon_{\mathrm{H,max}}$ is rather large on an absolute scale, reaching values as high as 6.5%. Assuming that the in-plane and out-of-plane lattice expansions are the same, the film appears to expand and contract by a large amount without an apparent loss of adhesion to the substrate.

C. Hydrogen-hydrogen and hydrogen-metal interaction

From the solubility isotherms the H-H interaction and H-metal interaction can be derived. First it should be noted that the Pd cap layer does not affect the equilibrium solubil-

ity conditions for the Nb films. This can be easily seen by the equilibrium of the chemical potentials for the free hydrogen gas and hydrogen in the metals,

$$\mu_{H_2} = 2\mu_{Pd(H)} \tag{7}$$

and

$$\mu_{Pd(H)} = \mu_{Nb(H)}, \tag{8}$$

yielding

$$\mu_{H_2} = 2\mu_{Nb(H)}. \tag{9}$$

The factor of 2 takes into account the dissociation of the H_2 molecule before entering the metal. Here the chemical potential of the free hydrogen gas μ_{H_2}, as long as it behaves ideally, can be expressed as

$$\mu_{H_2} = -U_{H_2} + k_B T \ln\left(\frac{p}{p_0}\right), \tag{10}$$

where U_{H_2} is the dissociation energy of H_2 (4.46 eV), k_B is the Boltzmann constant, and p_0 is given by

$$p_0 = \frac{(k_B T)^2 \theta}{\hbar}\left(\frac{k_B T m_{H_2}}{2\pi\hbar^2}\right)^{3/2}. \tag{11}$$

Here m_{H_2} is the mass of the H_2 molecule, and θ is the moment of inertia. Following Fukai,[1] we define a standard chemical potential via

$$\mu^{st}_{H_2} = -U_{H_2} + k_B T \ln\left(\frac{p^{st}}{p_0}\right), \tag{12}$$

where

$$p^{st} = p^{st}_0(T^\star) = 10^5 \ \text{Pa}. \tag{13}$$

Using the standard chemical potential, the chemical potential of the H_2 gas can be written as

$$\mu_{H_2} = \mu^{st}_{H_2} + k_B T \ln\left(\frac{p}{p_0(T^\star)}\right). \tag{14}$$

For the monatomic lattice gas, the chemical potential is given by

$$\begin{aligned}\mu_\alpha &= h_\alpha - TS_\alpha - uc_H + k_B T \ln\left(\frac{c_H}{r - c_H}\right)\\ &= \mu^{st}_\alpha - uc_H + k_B T \ln\left(\frac{c_H}{r - c_H}\right).\end{aligned} \tag{15}$$

The subscript α indicates the state of hydrogen in the metal as a disordered lattice gas. Here h_α is the partial enthalpy, which is the energy gained by dissolving a hydrogen atom in the metal matrix, TS_α is the change of the free energy from the free gas phase to the lattice-gas phase, c_H is the hydrogen concentration defined as the number ratio of the hydrogen atoms to the metal atoms per unit volume, and r is the maximum hydrogen concentration which can be reached in the disordered α or α' phase. r is determined by the short repulsive H-H interaction. Often r is set to 1, corresponding to a maximum hydrogen concentration in the α' phase of 100%. This is, however, unrealistic at least for lower hydrogen pressures up to 100 kPa, where $r = 2c_{H,c}$ appears to hold well. At higher pressures, a correction of r may be necessary. Finally, u represents the H-H interaction mediated by a long-range elastic strain field in the sample.[7] Here we assumed that u is a constant, and that the attractive H-H interaction is linearly proportional to the hydrogen concentration. This may be a oversimplification. Strictly speaking, u consists of two contributions, an elastic part and an electronic part,

$$u = u_{elast} + u_{elec}. \tag{16}$$

Only the elastic part may be constant, whereas the electronic part depends on details of the H - 1s and Nb - 4d band overlap and band filling.[26] Neglecting the weak concentration dependence of u in the following analysis, we write the H-H attractive interaction as uc_H.

Considering the equilibrium condition Eq. (9) and combining Eqs. (14) and (15), the external H_2 vapor pressure is related to the internal H concentration via

$$k_B T \ln\left(\frac{p}{p_0(T^\star)}\right) = -\mu^{st}_{H_2} + 2\mu^{st}_\alpha - 2uc_H + 2k_B T \ln\left(\frac{c_H}{r - c_H}\right). \tag{17}$$

Solving for the external hydrogen pressure yields

$$\begin{aligned}p_{H_2} &= p_0(T^\star)\left(\frac{c_H}{r - c_H}\right)^2 \exp\left(\frac{-(\mu^{st}_{H_2} - 2\mu^{st}_\alpha)}{k_B T}\right)\exp\left(-\frac{2uc_H}{k_B T}\right)\\ &= p_0(T^\star)\left(\frac{c_H}{r - c_H}\right)^2 \exp\left(\frac{-\Delta\mu}{k_B T}\right)\exp\left(-\frac{2uc_H}{k_B T}\right),\end{aligned} \tag{18}$$

where we have set

$$\mu^{st}_{H_2} - 2\mu^{st}_\alpha = \Delta\mu. \tag{19}$$

Since we cannot measure the hydrogen concentration on an absolute scale, we replace

$$\frac{c_H}{r - c_H} = \frac{\varepsilon_H}{\varepsilon_{H,max} - \varepsilon_H}, \tag{20}$$

where the common conversion factor f drops out, and we obtain

$$p_{H_2} = p_0(T^\star)\left(\frac{\varepsilon_H}{\varepsilon_{H,max} - \varepsilon_H}\right)^2 \exp\left(\frac{-\Delta\mu}{k_B T}\right)\exp\left(-\frac{6(u/f)\varepsilon_H}{k_B T}\right). \tag{21}$$

For fitting this expression to the measured isotherms we have three free parameters, including $\varepsilon_{H,max}$, $\Delta\mu$, and u/f. $\Delta\mu$ can be determined independently in the small concentration limit, where the H-H interaction may be neglected. In this limit we can write

$$p_{H_2} = p_0(T^\star)\left(\frac{\varepsilon_H}{\varepsilon_{H,max} - \varepsilon_H}\right)^2 \exp\left(\frac{-\Delta\mu}{k_B T}\right). \tag{22}$$

We cannot use the slope of a usual Arrhenius plot of $\ln(p)$ versus $1/T$ in order to derive $\Delta\mu$, since $\Delta\mu$ contains temperature dependent factors. Therefore we used $\Delta\mu$ as a fit parameter. The best fit parameters are listed in Table II.

TABLE II. Fit parameters derived from the solubility isotherms for the different Nb film thicknesses and temperatures.

D_{Nb} (nm)	T (K)	$\Delta\mu$ (eV)	u/f (eV)	$\varepsilon_{H,max}$	u (eV) $f=0.174$	T_c (K) fit	C.W.
32	473	0.22	0.47	0.068	0.08		
	523	0.19	0.40	0.069	0.07	254	275
	573	0.12	0.43	0.065	0.08		
78	473	0.21	0.80	0.057	0.14		
78	523	0.18	0.77	0.056	0.13	390	340
	573	0.12	0.83	0.055	0.15		
140	473	0.21	0.93	0.051	0.16		
	523	0.18	0.93	0.049	0.16	387	386
	573	0.16	0.93	0.050	0.16		
527	473	0.20	1.00	0.048	0.17		
	523	0.17	0.96	0.047	0.17	405	437
	573	0.11	1.00	0.046	0.17		

These values, which contain contributions from the enthalpy of solution and from the entropy change, are essentially the same as for H in bulk Nb. As expected, they depend on the temperature but not appreciably on the film thickness. The second fit parameter is the ratio u/f. However $\varepsilon_{H,max}$ can easily be taken from the x-ray data. In Fig. 4 the solid lines represent best fits of Eq. (21) to the isotherms using the fit parameters listed in Table II. For the ratio u/f we find values from 0.4 to 1.0 for films from 32 to 527 nm, respectively. u/f depends only on the film thickness but not on the temperature.

Using the fit parameters in Table II, either u or f can be derived, making assumptions about the other factor. For instance, using the bulk value for $f=0.174$, we find that the H-H interaction energy varies from 0.08 eV/atom for the thinnest film to 0.17 eV/atom for the thickest film. These interaction energies should be compared with bulk values, which vary in the literature between 0.24 and 0.41 eV/atom.[1]

For the bulk, the H-H interaction energy can be estimated either from the volume expansion or from the critical temperature of the α-α' phase transition, corresponding to the critical temperature for the incoherent phase transition. Thus, in the incoherent or strain-free limit the H-H interaction energy per H atom is given by[10]

$$u=\eta K_0\frac{(\Delta v)^2}{\Omega}, \tag{23}$$

where K_0 is the bulk modulus, and η takes short-range elastic and electronic repulsions into account. Experimentally, $\eta\approx 0.43$. Then with the bulk modulus of Nb (= 170 GPa) we find for u = 0.25 eV/atom. The bulk critical temperature is related to the H-H interaction via

$$k_B T_c=\tfrac{1}{4}ur. \tag{24}$$

With $T_c=444$ K, and $r=0.62$ we find again for u = 0.25 eV/atom. In the present thin films the H-H interaction shows a strong thickness dependence but no temperature dependence. Furthermore, the u values are systematically reduced as compared to the bulk even for the thickest film. In Table II we listed the interaction energies, and in Fig. 7 they are plotted as a function of the Nb film thickness. The solid line in Fig. 7 shows a fit to the data points using an expression from the finite-size scaling theory, as discussed in Sec. V B. Assuming that the correct conversion factor f has been used in this analysis, the data reflect a constant shift of the attractive H-H interaction to lower values for all film thicknesses. This downward shift may be the result of the elastic boundary condition. Our results on the reduced H-H interaction in thin films is in general agreement with the observations of Steiger, Blässer, and Weidinger.[5] However, concerning the systematics of the dependence and the quantitative values, some differences may be noticed.

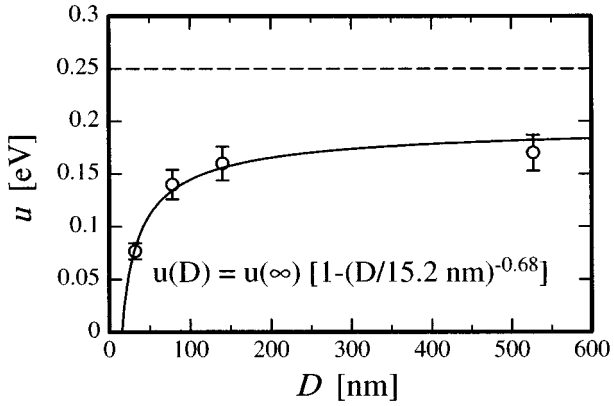

FIG. 7. The hydrogen-hydrogen interaction energy u is plotted vs the Nb film thickness. The interaction energy shows the same thickness dependence as the critical temperature shown in Fig. 9. The solid line describes the thickness dependence using finite-size scaling theory. The horizontal dashed line indicates the interaction energy in bulk Nb. Note that in the thin films the interaction energies are systematically shifted to lower values as compared to the bulk.

D. Thickness dependence of the critical temperature

The critical temperature for the α-α' transition in the thin films can be derived using two different approaches. In the first approach we take the slope of the isotherms at the inflection points, which follow a Curie-Weiss law:

$$\left(\frac{d\mu}{d\varepsilon_H}\right)^{-1}(c_H=c_{H,c})=\frac{C}{T-T_c}. \tag{25}$$

Usual Curie-Weiss plots for the different film thicknesses are shown in Fig. 8, from which the critical temperatures are obtained by extrapolation. The solid lines are least-square fits to the slopes of the isotherms.

In the second approach we estimate T_c from the interaction energies u as determined by the fits to the measured isotherms. According to Eq. (24),

$$T_c=\frac{u}{4k_B}r=\frac{u}{4k_B}(3/f)\varepsilon_{H,max}. \tag{26}$$

Using the bulk value for f, we find T_c values which are in good agreement with the critical temperatures derived from the Curie-Weiss plot. Therefore, using the bulk f factor may be justified in the present case. The T_c's evaluated from both

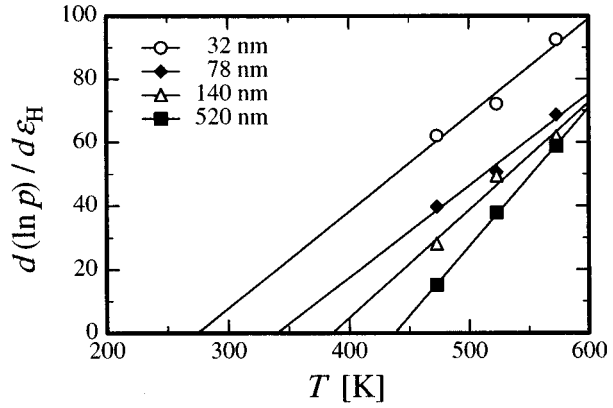

FIG. 8. The slope of the isotherm at the inflection point is plotted as a function of the temperature, showing a Curie-Weiss behavior. The intercepts of the solid lines with the temperature axis defines the critical temperature T_c for a specific film thickness.

approaches are plotted in Fig. 9. They clearly show a strong dependence on the film thickness. Unlike the interaction energy u, the T_c values steadily approach the bulk value for large thicknesses. The reason for this difference is the fact that the smaller u values are partially compensated for by higher r values.

For the crossover from three to two dimensions finite-size scaling theory predicts a dependence of the critical temperature on the linear dimension of the system according to[27]

$$\frac{T_c(D)-T_c(\infty)}{T_c(\infty)}=\left(\frac{D}{D_0}\right)^{-\lambda}. \tag{27}$$

Here $T_c(\infty)=444$ K, and $T_c(D)$ is the critical temperature for the film of thickness D with D_0 as a fit parameter. The shift exponent λ is related to the critical exponent ν for the correlation length ξ ($\xi=\xi_0\{[T_c(D)-T_c(\infty)]/T_c(\infty)\}^{-\nu}$) via $\lambda=1/\nu$. The best fit of the expression in Eq. (27) to the experimental critical temperatures is shown by the solid line in Fig. 8. From this fit we obtain a shift exponent $\lambda = 0.73$. For the interaction energy u we applied the same expression to fit the thickness dependence, and find a shift exponent of 0.68 (see the solid line in Fig. 7). Within the limits of the uncertainty the shift exponents for T_c and u can be considered identical.

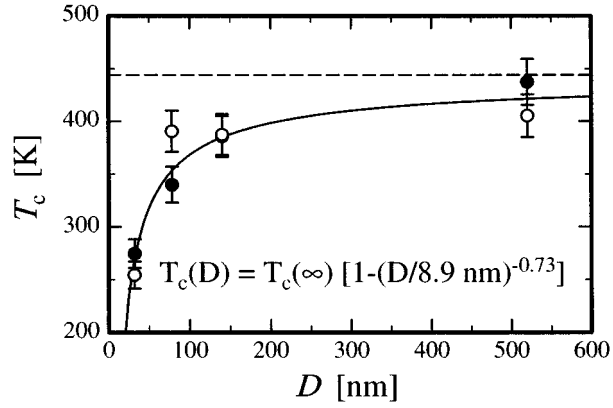

FIG. 9. The critical temperatures for the α-α' phase transition are plotted as a function of the Nb film thickness. The closed circles represent values from the Curie-Weiss plot shown in Fig. 7, and the open circles are calculated critical temperatures from the fit parameter u to the solubility isotherms, where u is the hydrogen-hydrogen interaction. The solid line shows a fit according to finite size scaling theory for the critical temperature. The dashed horizontal line indicates the bulk critical temperature.

Assuming that hydrogen in Nb films behaves like a three-dimensional Ising model, $\nu = 0.64$, and thus $\lambda = 1.56$ is predicted.[28] Thus there is a rather large discrepancy between the model prediction and the experiment. On the other hand, hydrogen in metals exhibits a very long-range, macroscopic interaction mediated by the elastic strain field.[7] Therefore a molecular-field approximation may be more appropriate for a description of the critical behavior of H in Nb. In this approximation, $\nu = 0.5$ and $\lambda = 2$,[28] which again is quite far from the experimental value. The obvious deviations from model predictions may be an indication that finite-size scaling is not a good description of the present thickness dependence. The small value found for λ expresses the fact that deviations from bulk properties set in at rather large Nb film thicknesses. For instance, at $D_{Nb} = 100$ nm the critical temperature drops by about 20%. This should be compared to magnetic thin films where a similar drop of T_c is observed for thicknesses which, however, are about two orders of magnitude thinner than in our case.[29] Although this may express the difference in the range of the elastic and magnetic interactions, we believe that the lowering of the critical temperature for the α-α' transition is rather due to the elastic boundary condition provided by the rigid substrate. In films of decreasing thickness, critical fluctuations of macroscopic density modes may be excited which are of decreasing wavelengths, and which are associated with lower and lower spinodal temperatures.

Extrapolating the critical temperatures to smaller thicknesses, we find that T_c drops below room temperature for thicknesses smaller than 30 nm, and that T_c becomes zero below 4 nm. This may also have practical implications.

VI. CONCLUSIONS

By *in situ* x-ray measurements we have determined the solubility isotherms for hydrogen in niobium thin films as a function of the film thickness and for hydrogen pressures up to 10^5 Pa. The pristine (110)-oriented Nb films are of high structural quality grown by molecular-beam epitaxy on $Al_2O_3(1120)$ substrates. They were capped with a thin Pd overlayer for oxidation protection and for enhancing the hydrogen diffusivity across the surface barrier even at rather low temperatures. After loading, the structural coherence breaks up in smaller domains, and the mosaicity increases considerably. The solubility isotherms react sensitively on the film thickness. The maximum lattice parameter change observed in saturation reaches values as high as 6.8% for the thinnest sample. In spite of this large change, the adhesion of the Nb film to the substrate must still be sufficient, since no peeling off of the film was observed. The maximum lattice parameter change scales inversely with the film thickness, indicating a strong surface effect. From fits to the measured isotherms, H-H interaction energies can be estimated which

decrease with decreasing film thickness, and furthermore exhibit a systematic reduction as compared to the bulk interaction energy by more than 20%. The critical temperature shows the same thickness dependence, although it approaches the bulk critical temperature of 444 K for large film thicknesses. Most likely, the strong thickness dependence of both, the H-H interaction energy and the critical temperature is due to the elastic boundary condition provided by the rigid substrate allowing macroscopic hydrogen density modes to be excited with decreasing wavelength as the film becomes thinner. Fits of the critical temperature to an expression provided by finite-size scaling theory yields shift exponents which are in strong contrast to exponents expected for molecular field or Ising-type phase transitions.

ACKNOWLEDGMENTS

We would like to thank R. Griessen and A. Weidinger for valuable discussions, P. Bödeker, I. Zoller, and K. Theis-Bröhl for their help during the sample preparation, and L. Borucki for the RBS measurements. This work was supported by the Bundesministerium für Bildung und Forschung under Contract No. ZA4BC1, and the Human Capital and Mobility program, which is gratefully acknowledged.

[1] Yuh Fukai, *The Metal-Hydrogen System*, Springer Series in Materials Science Vol. 21 (Springer-Verlag, Berlin, 1993).
[2] H. Zabel and A. Weidinger, Comments Condens. Matter. Phys. **17**, 239 (1995)
[3] F.A. Frazier and R. Glosser, J. Less-Common Metals. **74**, 89 (1980).
[4] S. Moehlecke, C.F. Majkrzak, and M. Strongin, Phys. Rev. B **31**, 6804 (1985).
[5] J. Steiger, S. Blässer, and A. Weidinger, Phys. Rev. B **49**, 5570 (1994).
[6] G. Reisfeld, N.M. Jisrawi, M.W. Ruckman, and M. Strongin, Phys. Rev. B **53** , 4974 (1996).
[7] H. Wagner and H. Horner, Adv. Phys. **23**, 587 (1974).
[8] H. Zabel and J. Peisl, Phys. Rev. Lett **42**, 511 (1979).
[9] H. Zabel and J. Peisl, Acta Metal. **28**, 589 (1980).
[10] H. Wagner, in *Hydrogen in Metals I*, edited by G. Alefeld and J. Völkl, Topics in Applied Physics Vol. 28 (Springer-Verlag, Berlin, 1978).
[11] S.M. Durbin, J.E. Cunningham, J.E. Mochel, and C.P. Flynn, J. Phys. F **11**, L223 (1981).
[12] K. Bröhl, P. Bödeker, N. Metoki, A. Stierle, and H. Zabel, J. Cryst. Growth **127**, 682 (1993).
[13] J. Mayer, C.P. Flynn, and M. Rühle, Ultramicroscopy **33**, 51 (1990).
[14] P. Sonntag, W. Donner, N. Metoki, and H. Zabel, Phys. Rev. B **49**, 2869 (1994).
[15] L.G. Parratt, Phys. Rev. Lett. **95**, 359 (1954).
[16] L. Névot and P. Croce, Rev. Phys. Appl. **15**, 761 (1980).
[17] A. Stierle, P. Bödeker, A. Abromeit, K. Bröhl, and H. Zabel, J. Appl. Phys. **73**, 4808 (1993).
[18] P.M. Reimer, H. Zabel, C.P. Flynn, and J.D. Dura, Phys. Rev. B **45**, 11 426 (1992)
[19] P.F. Miceli, in *Semiconductor Interfaces, Microstructures and Devices: Properties and Applications*, edited by Z.C. Feng (Adam Hilger, Bristol, 1992).
[20] J. Peisl, in *Hydrogen in Metals I*, edited by G. Alefeld and J. Völkl, Topics in Applied Physics Vol. 28 (Springer-Verlag, Berlin, 1978).
[21] P.F. Miceli, H. Zabel, J.A. Dura, and C.P. Flynn, J. Mater. Res. **6**, 964 (1991).
[22] P.M. Reimer, H. Zabel, C.P. Flynn, A. Matheny, K. Rtley, J. Steiger, and A. Weidinger, Z. Phys. Chem. **181**, 367 (1993).
[23] A. Abromeit, R. Siebrecht, G. Song, H. Zabel, F. Klose, D. Nagengast, and A. Weidinger, J. Alloys Compounds (to be published).
[24] W.J.M. de Jonge, P.J.H. Bloemen, and F.J. A. den Broeder, in *Ultrathin Magnetic Structures I*, edited by J.A.C. Bland and B. Heinrich (Springer-Verlag, Berlin, 1994).
[25] B. Hjörvarsson, J. Ryden, E. Karlsson, J. Birch, and J.E. Sundgren, Phys. Rev. B **43**, 6440 (1991).
[26] R. Griessen and T. Riesterer, in *Hydrogen in Intermetallic Compounds I, Electonic, Thermodynamic, and Crystallographic Properties, Preparation*, edited by. L. Schlapbach, Topics in Applied Physics Vol. 63 (Springer-Verlag, Berlin, 1988).
[27] M.N. Barber, in *Phase Transitions and Critical Phenomena*, edited by C. Domb and J.L. Lebowitz, (Academic, London, 1983), Vol. 8.
[28] H.E. Stanley, *Introduction to Phase Transitions and Critical Phenomena* (Clarendon, Oxford, 1971).
[29] Yi Li and K. Baberschke, Phys. Rev. Lett. **68**, 1208 (1992).